Numerical Investigation of the Coulter Principle in a Hydrodynamically Focused Microfluidics

Muheng Zhang and Yongsheng Lian

***Abstract*—A numerical method is proposed to study the Coulter principle in a microfluidics where low-conductive suspended cells and a high-conductive sample stream are hydrodynamically focused by two low-conductive sheath streams. The diffusion phenomenon of the high-conductive sample stream was modeled by solving a convection-diffusion equation. The motion of the suspended cell was calculated by solving the coupled equations of motion and the Navier-Stokes equations. The electric field was calculated by solving the Laplace's equation. With the proposed method, the effects of cell size, electrode size and electrode position, and the sheath flow width on the measured signal variation were systematically studied. Our simulations showed that fluid diffusivity plays an important role in determining the signal variation. We also showed that the current sensitivity increases with the cell size and the electrode size but it decreases with the sheath flow width.**

***Index Terms*—Coulter principle, computational fluid dynamics, hydrodynamic focusing, current sensitivity.**

I. Introduction

Coulter counter is an analytical microfluidic instrument used to measure the size and concentration of biological cells or colloid particles suspended in electrolyte [1]. Fig. 1 shows the schematic of a microfluidic Coulter counter with three inlets and one outlet. In this configuration a high-conductive sample stream is injected from the middle inlet on the left with suspended cells. Two electrodes are mounted on the bottom of the channel and they are connected to a galvanometer to measure the current between the two electrodes. When a low-conductivity cell passes through the electric field by the two electrodes, it interrupts the electrical path and causes a decrease in the measured current. The number and size of the cells can be obtained by carefully analyzing the measured signals. Due to its simplicity and portability, various designs of micro-Coulter counters have been used in the fields of chemistry, biology, and medicine [2]-[7] .

In the configuration shown in Fig. 1, the high-conductive stream and low conductive cells are hydrodynamically focused by two low-conductive streams which are injected from the top and bottom inlets.

The use of hydrodynamic focusing in a micro-fluidic system offers many desirable outcomes. For example, it can control the motion of the suspended cells to prevent cells from coming into contact with the walls and reduce the background noise [8], [9]. Also, hydrodynamic focusing can control the width and position of the high-conductive stream for better signals [10] and allow the cell stream to be steered into different output channels [11].

In the design of microfluidic Coulter counter, it is critical to have an accurate correlation between the signal variation, and the number and size of cells. The multidisciplinary nature of the problem makes it difficult to find an accurate analytical solution. Furthermore, the measured signal is affected by the concentration of the sample stream which involves different scales (low diffusivity but high viscosity). Various studies have been reported using methods of different fidelities. Some early studies used simplified analytical models to predict the signal variation due to the presence of cells [12]-[14]. One drawback of these simplified models is that they only consider sphere-shaped cells moving along the center axis line. Reference [15] derived an analytical solution to predict the resistance variation. They concluded that the current sensitivity decreases as the electrode width increases. Their conclusion is based on a relatively large cell with diameter of about thirty percent of the channel width. In their study they ignored the mass diffusivity and assumed a uniform conductivity distribution.

Experimental work has been performed to understand factors affecting signal variation [16]-[19]. For example, [17] showed that if electrodes were fixed on the bottom surface of a micro channel, the resistance variation would increase if the aperture dimension decreased. Reference [18] and [19] designed and tested a microfluidic Coulter counter using the hydrodynamic focusing effect. They also derived an analytical formula to predict the electric resistance between the two coplanar electrodes.

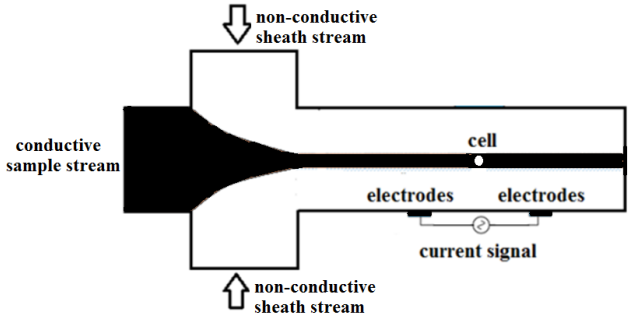

Fig. 1. Schematic of a 3-inlet micro coulter counter. The sample stream and cells are hydrodynamically focused for better signal quality.

The advancement of computational fluid dynamics (CFD) has made it possible to study microfluidics with numerical approaches. Recently, [20] studied the ion concentration distribution under the impact of two dimensional hydrodynamic focusing. They found that the focusing effect was increased when the angle increased from zero to ninety

Manuscript received January 21, 2014; revised May 10, 2014.

Yongsheng Lian is with University of Louisville, USA (e-mail: yongshenglian@gmail.com).

degrees. Reference [21] drew similar conclusions in their numerical study. Reference [22] simulated the electrical resistance variation when non-conductive cells pass through a micro-channel. Reference [23] numerically studied the impedance sensitivity in three different electrode configurations. They showed that face-to-face configurations had better current sensitivity than coplanar configurations. Reference [24] simulated the ion transport for micro size particles in a micro Coulter counter. Reference [25] showed that the normalized resistance variation was linearly dependent on the pore radius, but it decreased as the gap between the pores increased. Reference [26] and [27] used commercial software COMSOL to simulate the impedance change in a microfluidic Coulter counter. Reference [28] simulated the current changing in a microfluidic channel when the cell passed into the detection region. They showed that in a non-uniform electrical field the detected signal increases as the cell moves closer to the electrodes. Reference [29] simulated a microfluidic Coulter counter under DC driving. Both the hydrodynamic force and electro-kinetic force were considered. The simulation confirmed that the current pulse profile (amplitude, width, position) strongly depend on the particle size and flow condition.

In this paper, we proposed a numerical method to study the Coulter principle based on the design shown in Fig. 1. The proposed method differs from previous approaches in that it considers the fluid viscosity and the sample stream diffusivity which play critical roles in the signal variations but usually ignored in previous studies. In our approach the cell motion is calculated by closely coupling the Navier-Stokes equations with the equations of motion. Furthermore, the cell size in our study is relatively small with respect to the channel width. The paper is structured as follows: first, we present the proposed numerical methods; second, we validate the solvers; third, we present the numerical results; finally we make conclusions and suggestions.

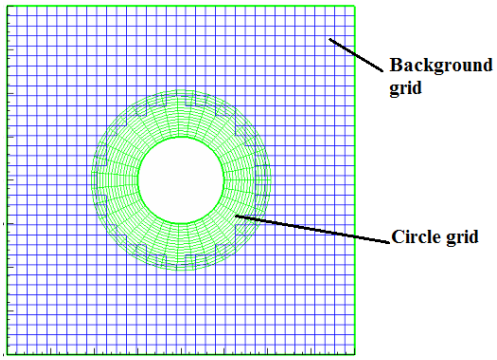

Fig. 2. Overlapping grids. Body-fitting grid is used around the circle and a cartesian grid is used as the background grid.

II. Governing Equations and Numerical Methods

A. Fluid Flow Governing Equations and Solver

The studied microfluidic Coulter counter has a velocity ranging from 0.1 cms-1 to 1 cms-1. The channel diameter is between 50 μm to 200 μm. For most cases involving liquid, this scale is well suited to the standard continuum description of transport processes [30]. The Reynolds number based on the fluid velocity and channel diameter is between 0.05 and 10. At this low Reynolds number flow remains laminar and incompressible. Flow behavior can be described by the unsteady incompressible Navier-Stokes equations

$$\nabla \bullet \vec{u} = 0 \tag{1}$$

$$\frac{\partial u}{\partial t} + \vec{u} \bullet \nabla \vec{u} = -\frac{\nabla p}{\rho} + \nu \nabla^2 \vec{u} \tag{2}$$

where ν is the kinematic viscosity, p is the pressure, $\vec{u}$ is the velocity vector, t is the time and ρ is the fluid density.

The governing equations (1) and (2) are solved using a pressure-Poisson method on overlapping grids. As discussed by [31], the overlapping moving grid method is suitable for moving boundary problems. As Fig. 2 shows, one circle grid overlaps with the background grid. Typically, boundary-conforming structured grids are used to achieve high-quality representations of the objects, and Cartesian grids are used as the background grid so that the efficiency inherent with such grids can be exploited. The irregular boundaries associated with standard Cartesian grid methods take the form of the interpolation boundary between overlapping grids. The interpolation points are located in the overlapping region to couple solutions from different domains. As an object moves, the grid moves with it, meaning that only the interpolation points need to be recalculated as opposed to regenerating the whole mesh. The convection terms, diffusion terms, and the pressure term are discretized using a second-order central difference scheme. The time integration is accomplished through a second accurate Adams-Bashforth-Moulton predictor-corrector method [32].

B. Sample Stream Concentration Equation and Solver

The electric field shown in Fig. 1 is affected by the concentration of the high-conductive sample stream. The concentration can be described by the following convection-diffusion equation,

$$\frac{\partial c}{\partial t} + \vec{u} \bullet \nabla c = k \nabla^2 c \tag{3}$$

where c is the concentration and k is the mass diffusivity. Though the concentration is affected by the flow field, the flow field is not affected by mass transfer. Hence, the convection-diffusion equation is decoupled from the Navier-Stokes equations. We use a second-order center difference scheme to discretize the convection and diffusion terms.

C. Electric Potential Distribution Equation and Solver

The electric potential distribution is described by the Laplace's equation,

$$\nabla \bullet (\sigma \nabla \phi) = 0 \tag{4}$$

where ϕ represents the potential and σ is the electrical conductivity. Special treatment is needed to solve Laplace's equation because the electrical conductivity is not continuous near the interface between the high-conductive stream and the low-conductive cell. To deal with the discontinuity in conductivity, the following central difference scheme is used. Equation (4) in the two-dimensional Cartesian coordinates has the following form:

$$\nabla \bullet (\sigma \nabla \phi) = \frac{\partial(\sigma \frac{\partial \phi}{\partial x})}{\partial x} + \frac{\partial(\sigma \frac{\partial \phi}{\partial y})}{\partial y} \quad (5)$$

where the first term on the right hand side is discretized as

$$\frac{\partial(\sigma \frac{\partial \phi}{\partial x})}{\partial x} = \frac{(\sigma \frac{\partial \phi}{\partial x})_{i+1/2,j} - (\sigma \frac{\partial \phi}{\partial x})_{i-1/2,j}}{dx} = \frac{\frac{\sigma_{i+1,j}+\sigma_{i,j}}{2}\frac{\phi_{i+1,j}-\phi_{i,j}}{dx} - \frac{\sigma_{i,j}+\sigma_{i-1,j}}{2}\frac{\phi_{i,j}-\phi_{i-1,j}}{dx}}{dx} \quad (6)$$

where $\sigma_{i,j}$ is the electrical conductivity at the grid point (i, j). The second term on the right side of (5) can be discretized similarly. This discretization leads to the system of equations

$$A\phi_{i,j} + B\phi_{i+1,j} + C\phi_{i-1,j} + D\phi_{i,j+1} + E\phi_{i,j-1} = 0 \quad (7)$$

where

$$A = 1 - w$$

$$B = w\frac{\sigma_{i+1,j}+\sigma_{i,j}}{2(dx)^2} / (\frac{\sigma_{i+1,j}+\sigma_{i,j}}{2(dx)^2} + \frac{\sigma_{i,j}+\sigma_{i-1,j}}{2(dx)^2} + \frac{\sigma_{i,j+1}+\sigma_{i,j}}{2(dy)^2} + \frac{\sigma_{j,i}+\sigma_{i,j-1}}{2(dy)^2})$$

$$C = w\frac{\sigma_{i,j}+\sigma_{i-1,j}}{2(dx)^2} / (\frac{\sigma_{i+1,j}+\sigma_{i,j}}{2(dx)^2} + \frac{\sigma_{i,j}+\sigma_{i-1,j}}{2(dx)^2} + \frac{\sigma_{i,j+1}+\sigma_{i,j}}{2(dy)^2} + \frac{\sigma_{j,i}+\sigma_{i,j-1}}{2(dy)^2})$$

$$D = w\frac{\sigma_{i,j+1}+\sigma_{i,j}}{2(dy)^2} / (\frac{\sigma_{i+1,j}+\sigma_{i,j}}{2(dx)^2} + \frac{\sigma_{i,j}+\sigma_{i-1,j}}{2(dx)^2} + \frac{\sigma_{i,j+1}+\sigma_{i,j}}{2(dy)^2} + \frac{\sigma_{j,i}+\sigma_{i,j-1}}{2(dy)^2})$$

$$E = w\frac{\sigma_{i,j}+\sigma_{i,j-1}}{2(dy)^2} / (\frac{\sigma_{i+1,j}+\sigma_{i,j}}{2(dx)^2} + \frac{\sigma_{i,j}+\sigma_{i-1,j}}{2(dx)^2} + \frac{\sigma_{i,j+1}+\sigma_{i,j}}{2(dy)^2} + \frac{\sigma_{j,i}+\sigma_{i,j-1}}{2(dy)^2})$$

Equation (7) can be solved using the successive over relaxation method [33].

The current density vector can be calculated by taking the gradient of the potential as follows:

$$\vec{J} = -\sigma \nabla \phi \quad (8)$$

and current can be calculated through integration.

III. Solver Validation

The fluid solver for (1), (2) and (3) have been validated by [34]. Here we only validate the solver for the electric potential equation. Two test cases are used for that purpose. In the first case we consider the electric potential distribution along a conductive bar. The bar is showed in Fig. 3. The bar has a dimensionless length of 1. Two scenarios are considered. In the first one, the unit-length bar has a uniform, dimensionless electrical conductivity of 1. In the second case, the electrical conductivity on the one dimensional bar is 0.1 between $0.222 < x < 0.322$ but is 1 everywhere else. Analytical solution exists in both cases. Fig. 4 compares the simulated and analytical solutions. In both cases the numerical results match the analytical ones.

In the second test we study the electric potential distribution in a two-dimensional (2D) field. As Fig. 5 shows, the 2D channel has a length of L and width of H. The channel has a uniform electrical conductivity. Two electrodes of equal size are mounted on the bottom surface. The rest boundary regions are set as the insulating boundaries. An analytical solution can be obtained using the Schwarz–Christoffel Mapping (SCM) when the channel length L approaches infinity [15]. We compares the numerical and analytical results along line *OB* (length=0.1). It is noted that the analytical solution is obtained for an infinitely long channel and simulations are based on finite length channels. Fig. 6 shows that the agreement between the analytical and numerical results is very good for both the three situations; the boundary has no significant effect on our results. The calculated potential distribution is shown in Fig. 7.

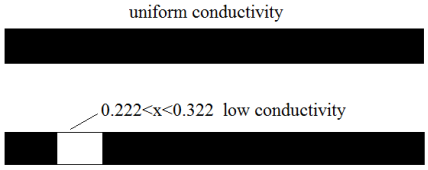

Fig. 3. Schematic of the 1D conductive bars. Top: 1D bar with uniform electrical conductivity; bottom: 1D bar with non-uniform conductivity, the red region has low conductivity.

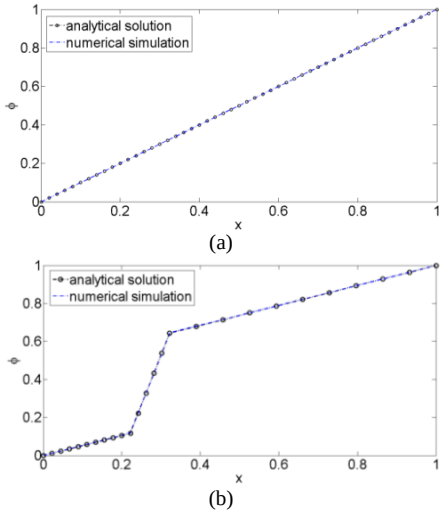

Fig. 4. Comparison of electric potential distribution along a bar with different conductivities. (a) with uniform conductivity, (b) with non-uniform conductivity.

IV. Numerical Results

In the next we study of effects of sample stream diffusivity, cell size, electrode size, and gap between the electrodes on

the current sensitivity. We choose dimensionless analysis and all the simulations are 2D. The channel length, electrode location and cell radius are normalized by the channel width. The diffusivity is reported as a dimensionless parameter.

A. The Impact of Diffusivity

Reference [15] proposed an analytical approach to predict the current variation due to the presence of a low-conductive cell in a high-conductive sample stream. In their study the diffusivity of the sample stream was ignored. Reference [34] showed that the diffusivity can alter the sample stream distribution.

To illustrate the impact of diffusivity we simulate a 3-inlet microfluidics channel which is shown in Fig. 8. Two low-conductive sheath flows are injected from the top and bottom inlets, the high-conductive sample flow is injected from the middle inlet.

In the simulation, uniform velocities are specified at the inlets and a zero gage pressure boundary condition is specified at the outlet. No-slip boundary conditions are applied on the channel walls and also on the moving cell. In the simulation the cell is inserted into the channel at the beginning of the simulation. For the study of the electric field we focus on the marked region in Fig. 8. The marked region has a length of two and a width of one. The electrodes are mounted at the bottom of the channel and are placed at the region of $x \in [6.4, 6.7]$ and $x \in [7.3, 7.6]$. The cell radius is 0.04. The conductivity of the cell is 0.1. At the inlets the conductivity of the sample stream and sheath streams is 1 and 0.1, respectively.

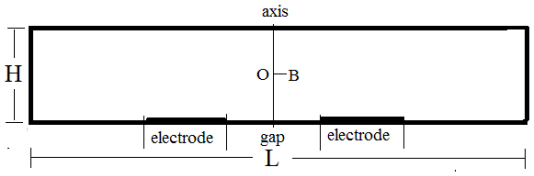

Fig. 5. Schematic of a finite length channel with electrodes mounted on the bottom.

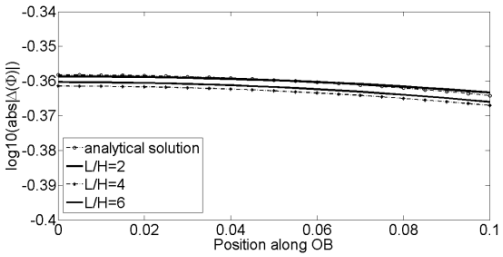

Fig. 6. Comparison of the electrical magnitude between numerical and analytical approaches.

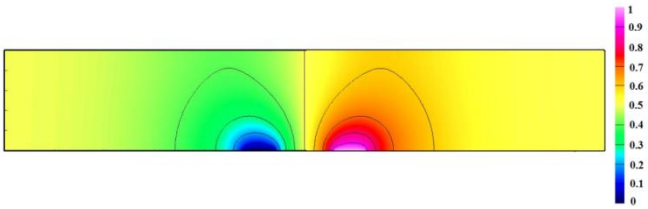

Fig. 7. Potential distribution in a 2D channel.

Two cases are simulated and compared. In the first case no diffusivity is considered and in the second case diffusivity (k=0.001 and Schmidt number, Sc=1000) is considered. Fig. 9 compares the conductivity distribution at x=7 with and without diffusivity. When diffusivity is considered the conductivity distribution profile is more spread out. Because the electrical field is affected by the conductivity distribution, the diffusivity also affects the current variation.

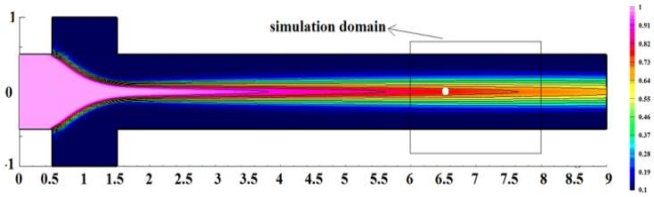

Fig. 8. Conductivity distribution in a Coulter counter. Sheath flows are injected from top and bottom inlets and high-conductive flow is injected from middle inlet.

The calculated current sensitivity with and without diffusivity is shown in Fig. 10. Following the work of [23], we use $\Delta I / I$ to represent the current sensitivity. Here I is the current when no cell exists, and ΔI is the current variation due to the cell. We can see that the current sensitivity is lower when diffusion is considered.

B. The Impact of Cell Size

To understand the impact of cell size we test three cells of different radii. The diffusivity of the sample stream is 0.001 for all the cases. The cell radius, r, is 2%, 3% and 4% of the channel width, respectively. The impact of cell size is shown in Fig. 11. It is clear that a larger cell leads to higher sensitivity and vice versa.

C. The Impact of Electrode Length and Gap between the Electrodes

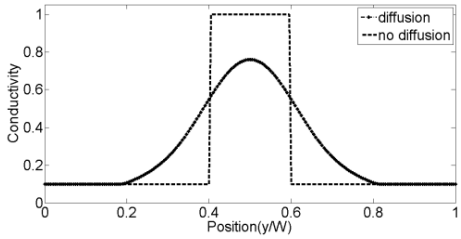

Fig. 9. Comparison of conductivity distribution of sample flows with and without mass diffusion at x=7.

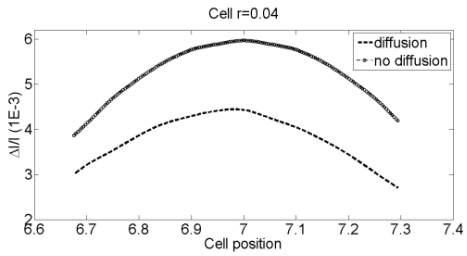

Fig. 10. Comparison of current sensitivity due to the presence of a low-conductivity cell with and without mass diffusion.

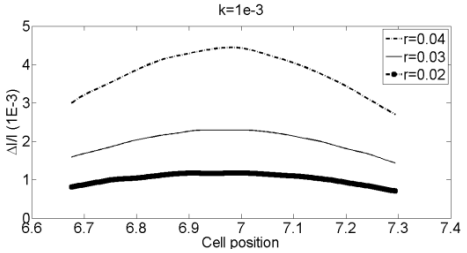

Fig. 11. Impact of cell size on the current sensitivity. A larger cell results in higher sensitivity.

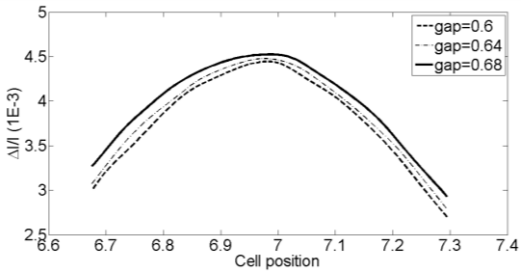

(a)

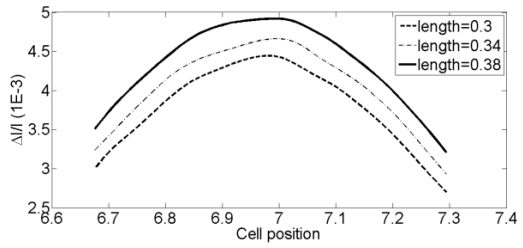

(b)

Fig. 12. Variation of current sensitivity with electrode length and gap. (a) impact of electrodes gap, (b) impact of electrodes length. In all the cases the two electrodes mounted on the bottom wall with the center at x=7.0.

The length of electrodes and the gap between them are two key parameters in the design of Coulter counters. We study their impact by systematically varying the electrode length and the gap between the electrodes. In all cases the center of the two electrodes is at x=7.0. Three different electrode lengths and three different gaps are tested and the simulation results are shown in Fig. 12. From those tests we conclude that the sensitivity increases with the electrode length and also with the gap.

D. The Impact of Electrodes Position

The current sensitivity is also affected by the location of the electrodes. Three electrode locations are selected and they are marked in Fig. 13. The cell radius is 0.03 for all the tests. In case A, the center of the two electrodes is centered at x=6.2, in case B it is centered at x=6.6, in case C, the center is at x=7. In all three cases the gap between the two electrodes is 0.6. The conductivity distribution at x=6.2, 6.6 and 7.0 are shown in Fig. 14. Due to the diffusion the conductivity distribution is more spread out further downstream at x=7.0 than the other two upstream.

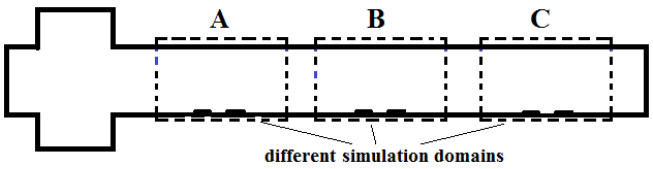

Fig. 13. Three different electrode locations along the channel. In case A, the center of the two electrodes is x=6.2, in case B the center is 6.6 and in case C the center is 7.0.

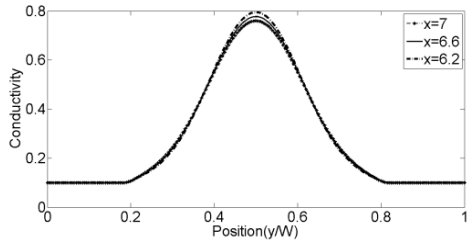

Fig. 14. Cross sectional conductivity distribution at the centers of region A, B and C.

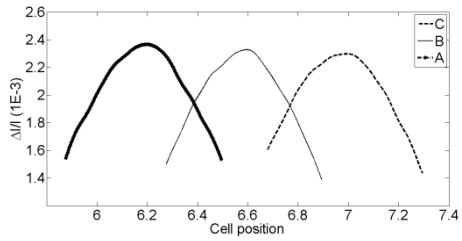

Fig. 15. Impact of electrode position on the current sensitivity.

The current sensitivity is shown in Fig. 15. It shows that when the electrodes are moved downstream, the current sensitivity decreases. This is because the sample stream is more spread out further downstream due to diffusion. Similar to the one shown in Fig. 10, a more concentrated sample stream results in higher current sensitivity than a less concentrated sample stream.

E. The Impact of Sheath Flow Rate

The width of the focused sample stream can be adjusted by changing the sheath flow rate. A high sheath flow rate leads to a narrow sample stream width and vice versa when we keep the total fluid rate as a constant. Here we choose the tested cell size r=0.03 and three different sheath flow rates (v=0.35, 0.36 and 0.37) to simulate the impact of sample stream width on the current sensitivity. The results are shown in Fig. 16. As the sheath flow rate increases, the sample stream width decreases, and the current sensitivity increases. This is because when the sample stream width decreases, the cell affects a relatively large portion of the conductive area and hence the sensitivity is high.

F. The Impact of Parallel Electrodes Distribution

The distribution of the electrodes can all be set as parallel. The electric potential distribution is shown in Fig. 17. Fig. 18 shows the current sensitivity (cell radius=0.04). We can see that the max current sensitivity is over 2% which is nearly five times than the results in Fig. 10(0.4%). The solution shows the current sensitivity under this parallel distribution is higher than that in the coplanar configuration. This conclusion is also confirmed by [15].

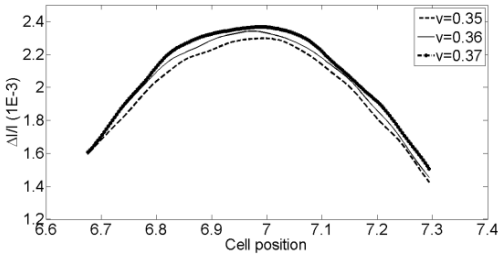

Fig. 16. Impact of the sheath stream rate on the current sensitivity. A higher sheath flow rate results in higher current sensitivity.

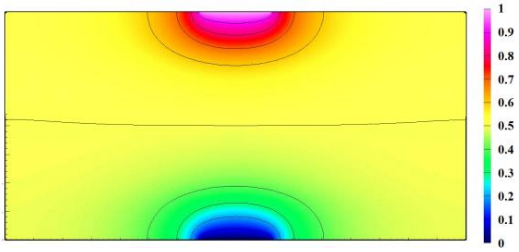

Fig. 17. Electric potential distribution under the parallel electrodes distribution.

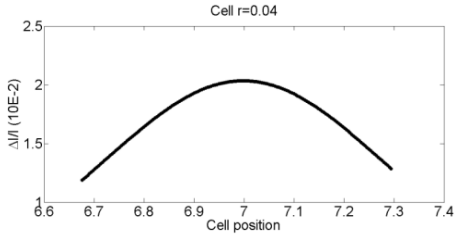

Fig. 18. Current sensitivity under the parallel electrodes distribution.

However, the parallel electrodes distribution is harder to fabricate than the coplanar electrodes distribution. Reference [35] showed that the parallel configuration needs two times of standard lift-off photo-lithography and sometimes the electrode is easy to fall off. On the other hand, Reference [19] showed that the fabrication of the coplanar electrodes distribution only needs one-time lithography and there is no electrode falling-off problem.

V. CONCLUSIONS

A numerical method is proposed to study the Coulter principle based on a three-inlets microfluidic Coulter counter. In this method both the fluid viscosity and mass diffusivity are considered. The cell motion is calculated by closely coupling the Navier-Stokes equations with the equations of motion. The accuracy of the numerical methods was validated by comparing against analytical solutions. From our simulations we concluded that diffusion lowers the current sensitivity. Our results also showed that the current sensitivity increases with cell size, electrode length, and the gap between the electrodes. We also showed that the sensitivity decreases as the sample stream width increases and as the electrodes are moved further downstream. The future work is to apply the proposed method to study three-dimensional problems.

ACKNOWLEDGMENT

The authors would like to thank the generous financial support from the Kentucky Science and Engineering foundation.

REFERENCES

[1]. L. P. Hsiang and G. M. Faeth, "Secondary drop breakup in the deformation regime," presented at 30th Aeropace Sciences Meeting & Exhibit, Reno, NV, 1992.
[2]. J. Atencia and D. J. Beebe, "Controlled microfluidic interfaces," *Nature*, vol. 437, pp. 648-655, September 2005.
[3]. G. Hairer, G. S. Parr, P. Svasek, A, Jachimowicz, and M. J. Vellekoop, "Investigations of micrometer sample stream profiles in a three-dimensional hydrodynamic focusing device," *Sensor Actuat B-Chem*, vol. 132, pp. 518-524, June 2008.
[4]. T. M. Squires and S. R. Quake, "Microfluidics: Fluid physics at the nanoliter scale," *Rev Mod Phys*, vol. 77, pp. 977-1026, October 2005.
[5]. H. A. Stone, A. D. Stroock, and A. Ajdari, "Engineering flows in small devices: Microfluidics toward a lab-on-a-chip," *Annu Rev Fluid Mech*, vol. 36, pp. 381-411, January 2004.
[6]. T. Vilkner, D. Janasek, and A. Manz, "Micro total analysis systems. Recent developments," *Anal Chem*, vol. 76, pp. 3373-3385, April 2004.
[7]. G. M. Whitesides and A. D. Stroock, "Flexible methods for microfluidics," *Phys Today*, vol. 54, pp. 42-48, June 2001.
[8]. G. B. Lee, C. C. Chang, S. B. Huang, and R. J. Yang, "The hydrodynamic focusing effect inside rectangular microchannels," *Journal of Micromechanics and Microengineering*, vol. 16, pp. 1024-1032, May 2006.
[9]. C. Xu, M. Wang, and X. Yin, "Three-dimensional (3D) hydrodynamic focusing for continuous sampling and analysis of adherent cells," *Analyst*, vol. 136, pp. 3877-3883, July 2011.
[10]. R. Scott, P. Sethu, and C. K. Harnett, "Three-dimensional hydrodynamic focusing in a microfluidic Coulter counter," *Review of Scientific Instruments*, vol. 79, April 2008.
[11]. G. B. Lee, C. I. Hung, B. J. Ke, G. R. Huang, and B. H. Hwei, "Micromachined pre-focused 1 x N flow switches for continuous sample injection," *Journal of Micromechanics and Microengineering*, vol. 11, pp. 567-573, July 2001.
[12]. R. W. Deblois and C. P. Bean, "Counting and Sizing of Submicron Particles by Resistive Pulse Technique," *Review of Scientific Instruments*, vol. 41, pp. 909-916, August 1970.
[13]. E. C. Gregg and K. D. Steidley, "Electrical counting and sizing of mammalian cells in suspension," *Biophysical journal*, vol. 5, pp. 393-405, July 1965.
[14]. J. C. Maxwell and J. J. Thomson, *A treatise on electricity and magnetism*, 3rd ed., Oxford: Clarendon, 1904, pp. 49-50.
[15]. T. Sun, N. G. Green, S. Gawad, and H. Morgan, "Analytical electric field and sensitivity analysis for two microfluidic impedance cytometer designs," *Iet Nanobiotechnol*, vol. 1, pp. 69-79, June 2007.
[16]. L. I. Berge, T. Jossang, and J. Feder, "Off-Axis Response for Particles Passing through Long Apertures in Coulter-Type Counters," *Meas Sci Technol*, vol. 1, pp. 471-474, June 1990.
[17]. J. H. Nieuwenhuis, F. Kohl, J. Bastemeijer, P. M. Sarro, and M. J. Vellekoop, "Integrated Coulter counter based on 2-dimensional liquid aperture control," *Sensor and Actuators B: Chemical*, vol. 102, pp. 44-50, September 2004.
[18]. R. R. Trujillo, O. C. Fernandez, M. Garrido, M. Arundell, A. Valencia, and G. Gomila, "High-speed particle detection in a micro-Coulter counter with two-dimensional adjustable aperture," *Biosensors and Bioelectronics* vol. 24, pp. 290-296, October 2008.
[19]. R. R. Trujillo, C. Mills, J. Samitier, and G, Gomila, "Low cost micro-Coulter counter with hydrodynamic focusing," *Microfluid Nanofluid*, vol. 3, pp. 171-176, 2007.
[20]. B. Ivorra, J. L. Redondo, J. G. Santiago, P. M. Ortigosa, and A. M. Ramos, "Two- and three-dimensional modeling and optimization applied to the design of a fast hydrodynamic focusing microfluidic mixer for protein folding," *Physics of Fluids*, vol. 25, 2013.
[21]. C. K. Olsen, J. Hoyland, and H. G. Rubahn, "Influence of geometry on hydrodynamic focusing and long-range fluid behavior in PDMS microfluidic chips," *Microfluidics and Nanofluidics*, vol. 12, pp. 795-803, 2012.
[22]. Z. P. Qin, J. Zhe, and G. X. Wang, "Effects of particle's off-axis position, shape, orientation and entry position on resistance changes of micro Coulter counting devices," *Meas Sci Technol*, vol. 22, March 2011.
[23]. D. Spencer and H. Morgan, "Positional dependence of particles in microfludic impedance cytometry," *Lab Chip*, vol. 11, pp. 1234-1239, April 2011.
[24]. Z. P. Qin, "Modeling of ion transport for micro/nano size particles in Coulter counter application," PhD dissertation, Dept. Me Eng., University of Akron, Akron, OH, 2009.
[25]. S. B. Cho, "Electrical resistance characterization of insulating membrane with multipore," *J Electroanal Chem*, vol. 629, pp. 69-72, April 2009.
[26]. Y. Wu, X. Han, J. D. Benson, and M. Almasri, "Micromachined Coulter counter for dynamic impedance study of time sensitive cells," *Biomed Microdevices*, vol. 14, pp. 739-750, Aug 2012.
[27]. J. H. Guo, T. S. Pui, A. R. A. Rahman, and Y. J. Kang, "Numerical Investigation of the Performance of Coulter Counter with Novel Structure," *International Journal of Information and Electronics Engineering*, vol. 2, pp. 885-888, November 2012.
[28]. J. Riordon, N. M. Catafard, and M. Godin, "Using the fringing electric field in microfluidic volume sensors to enhance sensitivity and accuracy," *Applied Physics Letters*, vol. 101, 2012.
[29]. J. Guo, T. S. Pui, A. R. Rahman, and Y. Kang, "3D numerical simulation of a Coulter counter array with analysis of electrokinetic forces," *Electrophoresis*, vol. 34. pp. 417-424, Febrary 2013.
[30]. H. A. Stone, and S. Kim, "Microfluidics: basic issues, applications, and challenges," *AIChE Journal*, vol. 47, pp. 1250-1254, June 2001.
[31]. N. A. Petersson, "Stability of pressure boundary conditions for Stokes and Navier-Stokes equations," *J Comput Phys*, vol. 172, pp. 40-70, September 2001.
[32]. W. D. Henshaw, "A 4th-Order Accurate Method for the Incompressible Navier-Stokes Equations on Overlapping Grids," *J Comput Phys*, vol. 113, pp. 13-25, July 1994.
[33]. J. D. Hoffman, *Numerical methods for engineers and scientists*, 2nd ed., New York: Marcel Dekker, 2001, pp. 65-67.

[34]. M. H. Zhang, Y. S. Lian, C. Harnett, and E. Brehob, "Investigation of Hydrodynamic Focusing in a Microfluidic Coulter Counter Device," *J Biomech Eng-T Asme*, vol. 134, August 2012.
[35]. D. K. Wood, M. V. Requa, and A. N. Cleland, "Microfabricated high-throughput electronic particle detector," *Review of Scientific Instruments*, vol. 78, 2007.

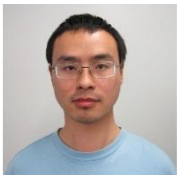

Muheng Zhang was born in China in 1983. He received the BS and MS degrees in mechanical engineering from Tongji University, China, 2009. At present he works in Caterpillar Inc. Peoria, IL and he is pursuing his PhD degree in the University of Louisville. His research areas include microfluidic, multiphase flow, heat transfer, aerodynamic, particle motion and transient flow.